The Astrophysical Journal, 825:109 (8pp), 2016 July 10 doi:10.3847/0004-637X/825/2/109

DOWNWARD CATASTROPHE OF SOLAR MAGNETIC FLUX ROPES

Quanhao Zhang[1,2], Yuming Wang[1,3], Youqiu Hu[1], and Rui Liu[1,4]
[1] CAS Key Laboratory of Geospace Environment, Department of Geophysics and Planetary Sciences, University of Science and Technology of China, Hefei 230026, China; zhangqh@mail.ustc.edu.cn
[2] Mengcheng National Geophysical Observatory, School of Earth and Space Sciences, University of Science and Technology of China, Hefei 230026, China
[3] Synergetic Innovation Center of Quantum Information & Quantum Physics, University of Science and Technology of China, Hefei, Anhui 230026, China
[4] Collaborative Innovation Center of Astronautical Science and Technology, China
Received 2016 March 15; revised 2016 April 28; accepted 2016 May 2; published 2016 July 7

ABSTRACT

2.5-dimensional time-dependent ideal magnetohydrodynamic (MHD) models in Cartesian coordinates were used in previous studies to seek MHD equilibria involving a magnetic flux rope embedded in a bipolar, partially open background field. As demonstrated by these studies, the equilibrium solutions of the system are separated into two branches: the flux rope sticks to the photosphere for solutions at the lower branch but is suspended in the corona for those at the upper branch. Moreover, a solution originally at the lower branch jumps to the upper, as the related control parameter increases and reaches a critical value, and the associated jump is here referred to as an upward catastrophe. The present paper advances these studies in three aspects. First, the magnetic field is changed to be force-free; the system still experiences an upward catastrophe with an increase in each control parameter. Second, under the force-free approximation, there also exists a downward catastrophe, characterized by the jump of a solution from the upper branch to the lower. Both catastrophes are irreversible processes connecting the two branches of equilibrium solutions so as to form a cycle. Finally, the magnetic energy in the numerical domain is calculated. It is found that there exists a magnetic energy release for both catastrophes. The Ampère's force, which vanishes everywhere for force-free fields, appears only during the catastrophes and does positive work, which serves as a major mechanism for the energy release. The implications of the downward catastrophe and its relevance to solar activities are briefly discussed.

Key words: Sun: coronal mass ejections (CMEs) – Sun: filaments, prominences – Sun: flares

1. INTRODUCTION

Coronal magnetic flux ropes are believed to have a close relationship with solar eruptive activities (e.g., Gibson & Fan 2006; Labrosse et al. 2010; Chen 2011), including prominence/filament eruptions, flares, and coronal mass ejections (CMEs), which are widely considered as different manifestations of a single physical process (e.g., Low 1996; Wu et al. 1999; Török et al. 2011; Zhang et al. 2014), corresponding to a sudden destabilization of the coronal magnetic configuration (Archontis & Török 2008). Flux ropes can be triggered to erupt by many different mechanisms such as magnetic reconnections and various instabilities (e.g., Antiochos et al. 1999; Chen & Shibata 2000; Moore et al. 2001; Kliem & Török 2006). It was also suggested by many authors that catastrophes could be responsible for the solar eruptive activities (Priest & Forbes 1990; Forbes & Priest 1995; Lin 2004; Zhang & Wang 2007). Catastrophes occur through a catastrophic loss of equilibrium as a control parameter of the magnetic system exceeds a critical value (Van Tend & Kuperus 1978; Forbes 1990; Isenberg et al. 1993). Here the control parameter characterizes the physical properties of the magnetic conguration. Any parameter can be selected as a control parameter provided that different values of this parameter will result in different configurations (Lin & van Ballegooijen 2002; Wang & Hu 2003; Su et al. 2011), and different kinds of control parameters correspond to different evolutionary scenarios (Kliem et al. 2014). During a catastrophe, magnetic free energy is quickly released and converted to kinetic and thermal energy (Chen et al. 2007). Catastrophes and instability are intimately related in the evolution of different magnetic systems (Kliem et al. 2014; Longcope & Forbes 2014).

Many solar eruptive activities originate from active regions (Benz 2008; Chen 2011) and Cartesian coordinates are widely used to investigate active region activities. In Cartesian coordinates, both analytical and numerical analyses have been performed to explore the catastrophic behaviors of flux ropes in a bipolar background field. If the bipolar field is completely closed, no catastrophe occurs for the flux rope of finite cross section (Hu & Liu 2000); only if the radius of the flux rope is small compared to the length scale of the photospheric magnetic field will there exist a catastrophe (Forbes & Isenberg 1991; Lin & van Ballegooijen 2002). During the catastrophe, the flux rope, originally attached to the photosphere, loses equilibrium at a critical value of the control parameter and reaches a new equilibrium levitating in the corona. In a partially open bipolar field, however, Hu (2001) found that a catastrophe also occurs for the flux rope of finite cross section. These studies imply that there are two branches of equilibrium states of a flux rope with a catastrophe: the lower branch and the upper branch. The flux rope sticks to the solar surface for solutions at the lower branch and levitates in the corona for those at the upper branch, with a vertical current sheet below it. The catastrophe mentioned above corresponds to a jump from the lower branch to the upper, and thus is called the "upward catastrophe" hereinafter.

All the previous studies only analyzed the upward catastrophe. Some questions still remain in theory: is there a catastrophe during which the flux rope falls back from the upper branch to the lower (called the "downward catastrophe" hereafter)? Will it also release magnetic free energy? To answer these questions, we follow the work by Hu (2001) to study the equilibrium solutions, but change to force-free fields. The motivations for using a force-free field structure rather than a

magnetostatic structure are as follows. First, the strong magnetic fields over active regions are usually considered to be force-free (Low 1977). Second, under force-free conditions, the system is dominated by magnetic fields, and its energy is limited to magnetic energy so as to substantially simplify the energy analysis (see Section 3.2). By analyzing the evolution of the equilibrium solutions versus the control parameters in Cartesian coordinates, the properties of the catastrophes in partially open bipolar background field under the force-free approximation are investigated. We mainly focus on the existence of the downward catastrophe, and the evolutions of the magnetic energy during the catastrophes. The sections are arranged as follows: the simulation methods are introduced in Section 2; the two kinds of catastrophe are demonstrated in Section 3.1; the variations of magnetic energy during upward and downward catastrophes are analyzed in Section 3.2; by summarizing the simulation results, the whole evolution of a flux rope in a partially open bipolar field is illustrated in Section 3.3; the mechanism by which magnetic energy is released is analyzed in Section 3.4; and the significance of catastrophe in both observational and theoretical analyses are discussed in Section 4.

2. BASIC EQUATIONS AND THE INITIAL AND BOUNDARY CONDITIONS

A Cartesian coordinate system is taken and the magnetic flux function is used here to denote the magnetic fields as follows:

$$\boldsymbol{B} = \nabla \times (\psi \hat{\boldsymbol{z}}) + B_z \hat{\boldsymbol{z}}, \tag{1}$$

and the 2.5-dimensional magentohydrodynamic (MHD) equations can be written in the non-dimensional form:

$$\frac{\partial \rho}{\partial t} + \nabla \cdot (\rho \boldsymbol{v}) = 0, \tag{2}$$

$$\frac{\partial \boldsymbol{v}}{\partial t} + \boldsymbol{v} \cdot \nabla \boldsymbol{v} + \nabla T + \frac{T}{\rho}\nabla \rho + \frac{2}{\rho \beta_0}(\triangle \psi \nabla \psi + B_z \nabla B_z + \nabla \psi \times \nabla B_z) + g\hat{\boldsymbol{y}} = 0, \tag{3}$$

$$\frac{\partial \psi}{\partial t} + \boldsymbol{v} \cdot \nabla \psi = 0, \tag{4}$$

$$\frac{\partial B_z}{\partial t} + \nabla \cdot (B_z \boldsymbol{v}) + (\nabla \psi \times \nabla v_z) \cdot \hat{\boldsymbol{z}} = 0, \tag{5}$$

$$\frac{\partial T}{\partial t} + \boldsymbol{v} \cdot \nabla T + (\gamma - 1) T \nabla \cdot \boldsymbol{v} = 0, \tag{6}$$

where ρ, $\boldsymbol{v}$, T, ψ correspond to the density, velocity, temperature, and magnetic flux function, respectively; B_z and v_z denote the z-component of the magnetic field and the velocity, parallel to the axis of the flux rope; g is the normalized gravity, $\beta_0 = 2\mu_0 \rho_0 R T_0 L_0^2/\psi_0^2 = 0.1$ is the characteristic ratio of the gas pressure to the magnetic pressure, where μ_0 is the vacuum magnetic permeability, and R is the gas constant. $\rho_0 = 3.34 \times 10^{-13}\,\mathrm{kg\,m^{-3}}$, $T_0 = 10^6\,\mathrm{K}$, $L_0 = 10^7\,\mathrm{m}$, and $\psi_0 = 3.73 \times 10^3\,\mathrm{Wb\,m^{-1}}$ are the characteristic values of density, temperature, length and magnetic flux function, respectively. The radiation and heat conduction in the energy equation have been neglected.

The initial corona is isothermal and static with

$$T_c \equiv T(0, x, y) = 1 \times 10^6\,\mathrm{K},$$
$$\rho_c \equiv \rho(0, x, y) = \rho_0 \exp^{-gy}. \tag{7}$$

The background field, assumed to be symmetrical relative to the y-axis, is a partially open bipolar magnetic field, which is calculated using the complex variable method (see Hu 2001). The positive and a negative surface magnetic charges are located at $y = 0$ within $5\,\mathrm{Mm} < x < 35\,\mathrm{Mm}$ and $-35\,\mathrm{Mm} < x < -5\,\mathrm{Mm}$, respectively. The computational domain is taken to be $0 \leqslant x \leqslant 300\,\mathrm{Mm}$, $0 \leqslant y \leqslant 300\,\mathrm{Mm}$, with symmetrical conditions used for the left side ($x = 0$). The lower boundary $y = 0$ corresponds to the photosphere. During the simulation, the top ($y = 300\,\mathrm{Mm}$) and right ($x = 300\,\mathrm{Mm}$) boundary conditions are fixed. Fixed boundary conditions greatly help to maintain the stability of the simulation. We have tried the simulations with computational domains of different sizes (e.g., $0 \leqslant x \leqslant 200\,\mathrm{Mm}$), and found that the size of the domain does not influence the existence of the catastrophes. Although the critical values of the control parameters at which the catastrophe takes place vary slightly with the domain size, the deviations are smaller than 10%. This indicates that the computational domain used here is large enough so that the influence of the boundary condition on the evolution of the magnetic system is almost negligible.

Starting from the background field, with the same procedures as in Hu & Jiang (2001), a magnetic flux rope emerges from the central area of the base, resulting in an equilibrium state with a flux rope sticking to the photosphere, i.e., a lower-branch solution, which is the initial state of our simulation (see Figure 1(a) in Hu & Jiang 2001).

With the initial and boundary conditions, Equations (2) to (6) are solved by the multi-step implicit scheme (Hu 1989) to allow the system evolve to equilibrium states. The relaxation method was used by Hu (2004) to obtain force-free equilibrium solutions in spherical coordinates. This method resets the temperature and density in the computational domain to their initial values, so that the pressure gradient force is always balanced everywhere by the gravitational force. Using the same method in Cartesian coordinates, we obtain force-free equilibrium solutions. Moreover, during the whole simulation, both numerical and physical magnetic reconnections are prohibited. In theory, ψ is constant along a current sheet. Any reconnection will reduce the value of ψ at the reconnection site. Therefore, by reassigning ψ with the initial value at each time step along the entire current sheet (if it exists), we keep ψ invariant, so that reconnections are completely prevented across the current sheet.

In this paper, we select the axial magnetic flux passing through the cross section of the flux rope, Φ_z, and the annular magnetic flux of the rope per unit length along the z-direction, Φ_p, which is simply the difference of ψ between the rope axis and the outer border of the rope, as the control parameters. The varying Φ_z and Φ_p represent the evolutionary scenarios, e.g., flux emergence and twisting/untwisting motions. If not changed manually, Φ_z and Φ_p of the rope should be maintained to be conserved, which is achieved by special numerical measures: following similar procedures proposed by Hu et al. (2003), a slight adjustment of B_z inside the flux rope and ψ at the rope axis is taken at the end of each time step. The evolution of the equilibrium solutions is described by the

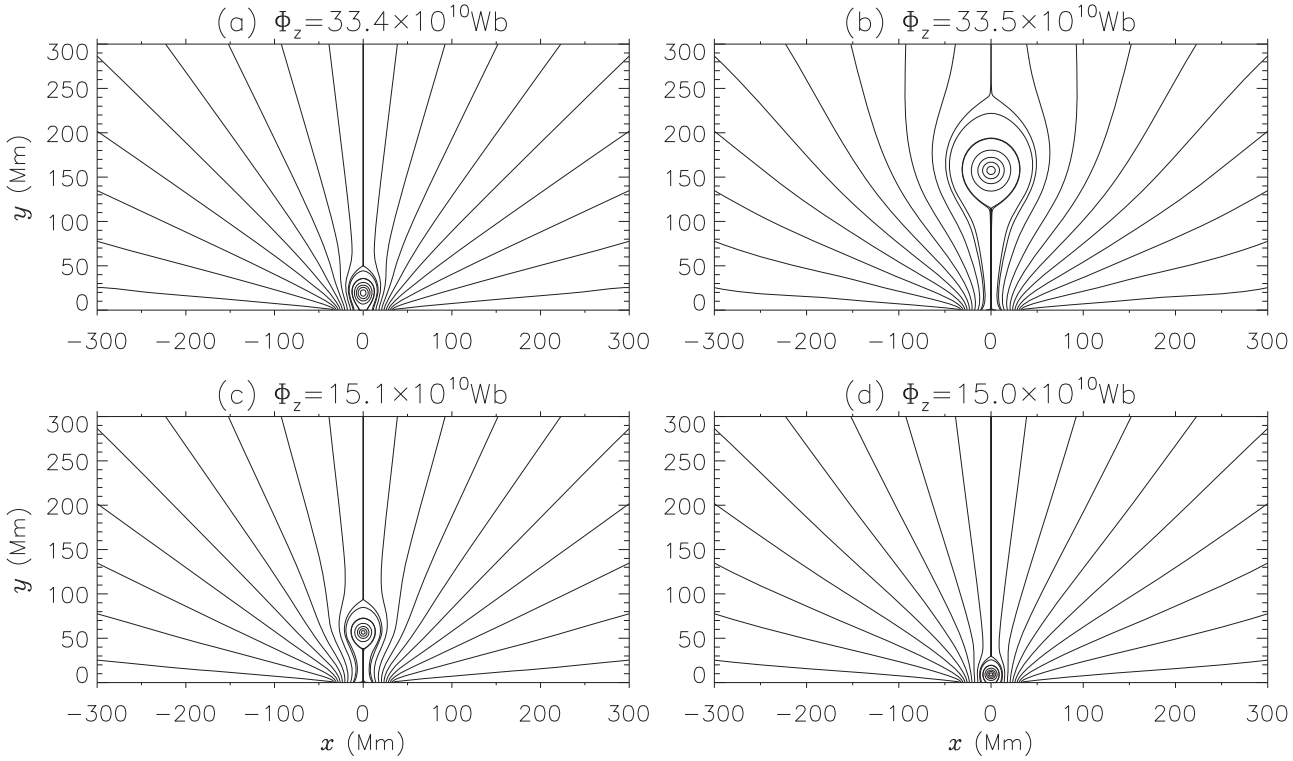

Figure 1. Magnetic configurations of the flux rope system (a) immediately before and (b) after the upward catastrophic point, and (c) immediately before and (d) after the downward catastrophic point. The annular flux is fixed to be $\Phi_p = 14.9 \times 10^3$ Wb m^{-1} for the system, whereas the axial flux Φ_z is taken as the control parameter.

geometric parameters of the flux rope, including the height of the rope axis, H, and the length of the current sheet below the rope, L_c. Note that at the lower branch, $L_c = 0$, and at the upper branch, L_c is finite.

3. SIMULATION RESULTS

3.1. Upward and Downward Catastrophes

Starting from the initial state, equilibrium solutions with different control parameters are calculated in the following way: from 0 to $100\tau_A$, Φ_z and Φ_p are linearly changed from the same initial values to target values (Φ_z^1, Φ_p^1), and from $100\tau_A$ to $200\tau_A$, the two fluxes are kept invariant until the magnetic system reaches an equilibrium state. Here $\tau_A = L_0^2\sqrt{\mu_0\rho_0}/\psi_0 = 17.4$ s is the typical Alfvén transit time. The final state of this calculation at $t = 200\tau_A$ is regarded as the equilibrium solution with (Φ_z^1, Φ_p^1). Similar calculations are repeated for different target values of Φ_z and Φ_p to obtain different equilibrium solutions.

First, in order to analyze the evolution of the equilibrium solutions versus Φ_z, we focus on the solutions with different Φ_z but the same $\Phi_p = 14.9 \times 10^3$ Wb m^{-1}. The geometric parameters describing these equilibrium solutions are plotted by the red dots in Figures 2(a) and (c). The flux rope keeps sticking to the photosphere for $\Phi_z < 33.5 \times 10^{10}$ Wb (see Figure 1(a)) and the equilibrium solutions remain at the lower branch. Once the control parameter reaches $\Phi_z = 33.5 \times 10^{10}$ Wb, however, the flux rope jumps to the equilibrium state at the upper branch, levitating in the corona, as shown in Figure 1(b). This indicates that a catastrophe with the flux rope jumping from the lower branch to the upper branch takes place, which is the upward catastrophe analyzed in previous studies, and the critical value of the control parameter Φ_z is called the upward catastrophic point: $\Phi_z^u = 33.5 \times 10^{10}$ Wb. Our simulation reveals that the upward catastrophe also occurs in partially open bipolar field under force-free approximations.

As mentioned above, all the previous studies only analyzed the upward catastrophe. Here are the questions to be considered: what will happen to the flux rope at the upper branch with decreasing Φ_z? Will the flux rope fall back to the lower branch? If so, will the flux rope fall back by a catastrophic jump or a continuous transition? To solve these problems, we start from the equilibrium solution at the upper branch obtained above (Figure 1(b)) and decrease Φ_z to calculate the equilibrium solutions at the upper branch with similar procedures, i.e., from 0 to $100\tau_A$ decrease Φ_z to a certain value and from $100\tau_A$ to $200\tau_A$ the system relaxes to an equilibrium state with the given Φ_z. Φ_p is still fixed to be 14.9×10^3 Wb m^{-1}. As shown by the blue dots in Figures 2(a) and (c), with decreasing Φ_z, the flux rope does not fall back to the lower branch at Φ_z^u, indicating that the upward catastrophe is an irreversible process. The simulation result reveals that the flux rope also remains suspended in the corona, and the associated equilibrium solutions remain at the upper branch, until $\Phi_z = 15.0 \times 10^{10}$ Wb (Figure 1(c)), at which point the flux rope suddenly falls back to the photosphere (Figure 1(d)). This indicates that there exists another kind of catastrophe, during which the flux rope falls down from the upper branch to the lower branch, i.e., a downward catastrophe. The downward catastrophic point is $\Phi_z^d = 15.0 \times 10^{10}$ Wb. Furthermore, we increase Φ_z again, but from the lower-branch solution immediately after the downward catastrophe (Figure 1(d)), to calculate equilibrium solutions with varying Φ_z, as shown by the black triangles in Figures 2(a) and (c). Similarly, the flux rope does not jump to the upper branch at Φ_z^d as well, indicating that the downward catastrophe is also an irreversible process.

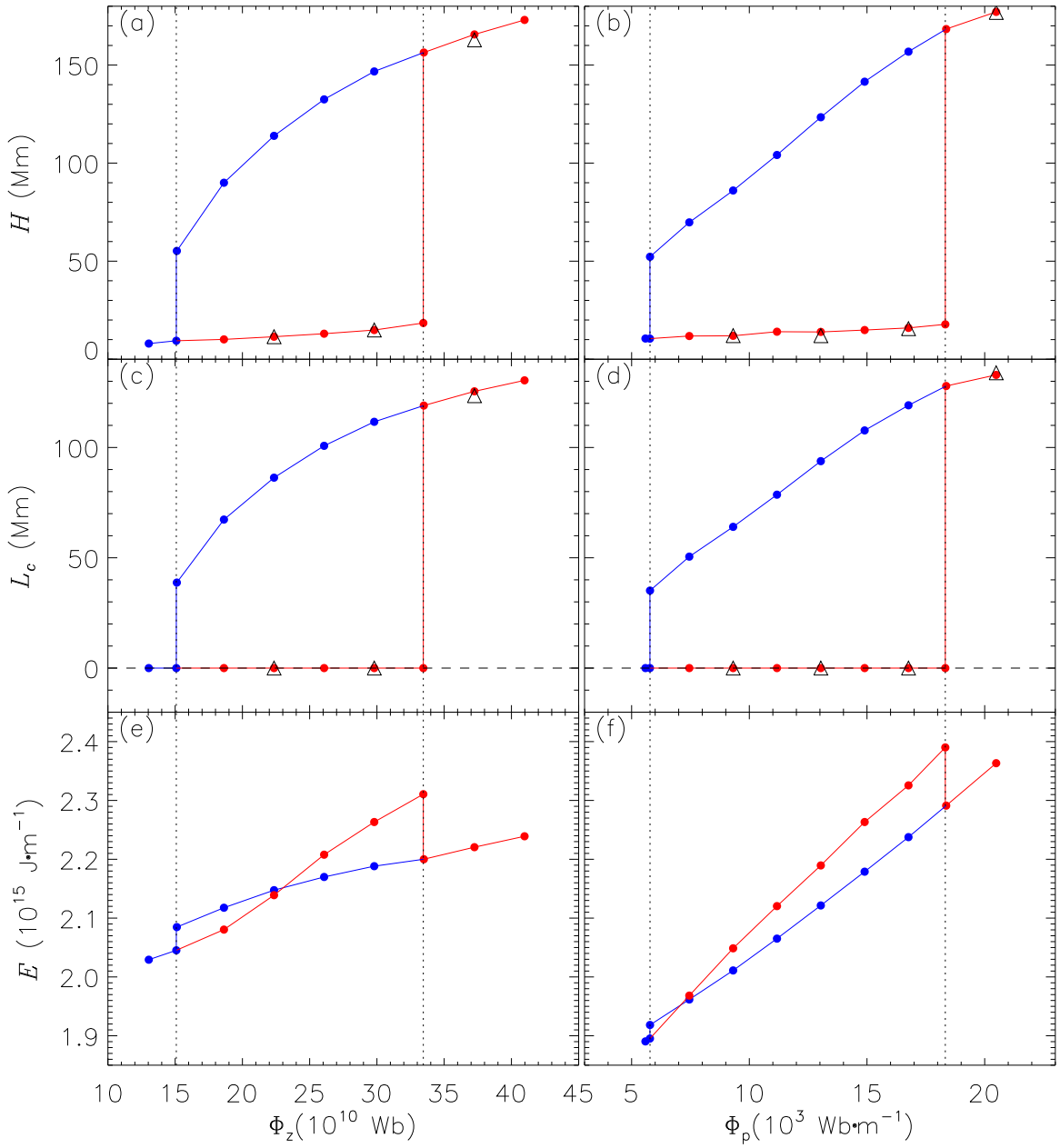

Figure 2. The height of the flux rope axis (H), the length of the current sheet below the rope (L_c), and the magnetic energy in the computational domain (E) are shown as functions of the control parameter Φ_z for $\Phi_p = 14.9 \times 10^3$ Wb m^{-1} in the left three panels, and as functions of the control parameter Φ_p for $\Phi_z = 29.8 \times 10^{10}$ Wb in the right three panels. The red dots represent equilibrium solutions, which are obtained by increasing the related control parameter, proceeding from the lower branch to the upper via the upward catastrophic point, whereas the blue dots represent those which are obtained by decreasing the related control parameter, proceeding from the upper branch to the lower via the downward catastrophic point. Finally, the solutions denoted by triangles are obtained from the product of the downward catastrophe and a monotonic increase of Φ_z, and they follow almost the same profile as the red dots do.

From Figures 2(a) and (c), it can be seen that the equilibrium solutions calculated from the solution immediately after the downward catastrophe (black triangles) follow almost the same profile as the red dots do. When Φ_z reaches the catastrophic point, an upward catastrophe takes place as before. Consequently, a circulation is formed by these two different kinds of catastrophes (see Section 3.3). The values of the catastrophic points are close to the observed magnetic fluxes of CMEs (e.g., Wang et al. 2015).

There are also upward and downward catastrophes when the annular magnetic flux Φ_p is taken to be the control parameter with fixed $\Phi_z = 29.8 \times 10^{10}$ Wb. By similar procedures as mentioned above, the evolution of equilibrium solutions versus Φ_p is obtained, as plotted in Figures 2(b) and (d). The meanings of the symbols are the same: red dots denote the process of searching for the upward catastrophe, blue for the downward catastrophe, and black triangles are the equilibrium states calculated from the state after the downward catastrophe has taken place. Both the upward and downward catastrophes exist and belong to irreversible processes. The upward catastrophic point is $\Phi_p^u = 18.4 \times 10^3$ Wb m^{-1}, and the downward catastrophic point is $\Phi_p^d = 5.78 \times 10^3$ Wb m^{-1}.

3.2. Evolution of the Magnetic Energy

As pointed out in Section 3.1, there exist upward and downward catastrophes; they are both irreversible processes, but the flux rope moves in opposite directions. Whether magnetic energy is released or stored during the downward catastrophe will help in understanding the nature of these two catastrophes. Since the magnetic energy per unit length along the z-axis is infinite for a partially open bipolar field in Cartesian coordinates, the evolution of magnetic energy has never been touched upon before. As an expedient measure, we evaluate the magnetic energy in the computational domain only, and think that it approximately represents the evolutionary tendency of the magnetic energy of the whole system. As long as the domain is sufficiently large in size, as we explained in Section 2, the conclusions obtained should be qualitatively correct.

The magnetic energy per unit length in the z-direction in the computational domain is calculated by:

$$E = \iint \frac{B^2}{2\mu_0} dxdy. \tag{8}$$

The evolutions of the magnetic energy within the domain are plotted in Figures 2(e) and (f) with Φ_z and Φ_p as the control parameters, respectively. Magnetic energy is released during both of the two catastrophes. It is natural that magnetic energy is always released during catastrophes: any catastrophe belongs to a spontaneous process in the absence of external influences, and the system must evolve to a state of lower energy after the catastrophe. We may conclude that, although different kinds of catastrophes could have different kinematic characters (e.g., in this paper the moving directions of the flux rope are opposite during the upward and downward catastrophes), a catastrophe should always correspond to a sudden energy release. By assuming that spatial scale in z-direction is the same as x-direction and y-direction, i.e., ~300 Mm, the released energy of the catastrophes is estimated to be: 3.3×10^{22} J for the upward catastrophe and 1.2×10^{22} J for the downward catastrophe with Φ_z as the control parameter; 3.0×10^{22} J for the upward and 6.9×10^{21} J for the downward with Φ_p as the control parameter. More magnetic energy is released for the upward catastrophe than the downward. It is revealed that the released magnetic energy during the catastrophes is of the order of 10^{22} J. It should be noted that the amount of the released energy is inversely proportional to the value of β_0, which is set to be 0.1 in this study. Larger amount of released magnetic energy can be obtained with smaller β_0. For example, if $\beta_0 = 0.001$, which is more proper for coronal situation (Amari & Luciani 1999), the released energy should be as large as $\sim 10^{24}$ J, which is comparable to the released energy of a medium flare.

3.3. A Cyclic Evolution of the Flux Rope System

The evolution of a flux rope in a partially open bipolar background field as discussed in Sections 3.1 and 3.2 is summarized in Figure 3, where h stands for the geometric parameter and λ the control parameter. There are two branches of equilibrium states for the flux rope: the lower branch ($D \sim A$ in Figure 3) and the upper branch ($C \sim B$ in Figure 3). The two branches are separated by the upward (from lower to upper branch) and downward (from upper to lower branch) catastrophes. The upward (downward) catastrophe is an irreversible but reproducible process, and it takes place when the solution jumps from the lower (upper) branch to the upper (lower) branch with increasing (decreasing) control parameter. Therefore, the two branches and the two catastrophes form a circulation, as shown by $D \rightarrow A \rightarrow B \rightarrow C \rightarrow D$ in Figure 3(a).

The evolution of magnetic energy (Figure 3(b)) is also a circulation consisting of the two branches and two catastrophes, but it is quite different from that of the geometric parameter (Figure 3(a)). At the lower branch ($D \rightarrow A$), magnetic energy is stored with increasing control parameter, whereas it is reduced during both upward and downward catastrophes, and during the shift of the solution along the upper branch from B to C as well. The constraint exerted by the background field on the flux rope is larger for solutions at the lower branch than that at the upper branch, so that the growth rate of the magnetic energy with λ, $dE/d\lambda$, is larger for lower-branch solutions than upper-branch solutions. Consequently, at the upward catastrophic point ($\lambda = \lambda_u$), the magnetic energy of the upper-branch solution is smaller than that of the lower-branch solution ($E_2 < E_1$), whereas at the downward catastrophic point ($\lambda = \lambda_d$), the opposite is true ($E_3 > E_4$). This provides the essential energy condition under which the downward catastrophe could occur.

3.4. Mechanism of Magnetic Energy Release During the Catastrophe

It is widely accepted that magnetic energy is released by magnetic reconnection in solar eruptive activities (Benz 2008; Shibata & Magara 2011). However, magnetic reconnections are prohibited during our simulation (see Section 2). There should be other mechanisms of magnetic energy release in addition to magnetic reconnection. By simulations in spherical coordinates, Chen et al. (2006) found that the magnetic force acting on the flux rope vanishes for equilibrium states, but becomes upward if the rope erupts after the upward catastrophe. As a result, the flux rope is expected to be accelerated by the Ampère's force. Here, we calculate the work done by Ampère's force during the catastrophe in the entire computational domain, so as to reveal the mechanism of magnetic energy release.

Figure 4 shows the temporal profiles of relevant geometric and physical parameters during a transition toward the equilibrium solutions immediately before and after the upward catastrophe, which correspond to (Φ_z, Φ_p) = (33.4×10^{10} Wb, 14.9×10^3 Wb m^{-1}) and (33.5×10^{10} Wb, 14.9×10^3 Wb m^{-1}), respectively. The first four panels show the geometric parameters, including H and L_c, whereas panels (e) and (f) show the magnetic energy. Finally, panels (g) and (h) depict the rate of doing work by Ampère's force, which is determined by:

$$\begin{aligned} W &= \iint \boldsymbol{j} \cdot \boldsymbol{E} dxdy \\ &= \iint -\boldsymbol{j} \cdot (\boldsymbol{v} \times \boldsymbol{B}) dxdy \\ &= \iint \left[\frac{1}{\mu_0} (\nabla \times \boldsymbol{B}) \times \boldsymbol{B} \right] \cdot \boldsymbol{v} dxdy, \end{aligned} \tag{9}$$

where $\boldsymbol{j}$ and $\boldsymbol{E}$ denote the current density and electric field.

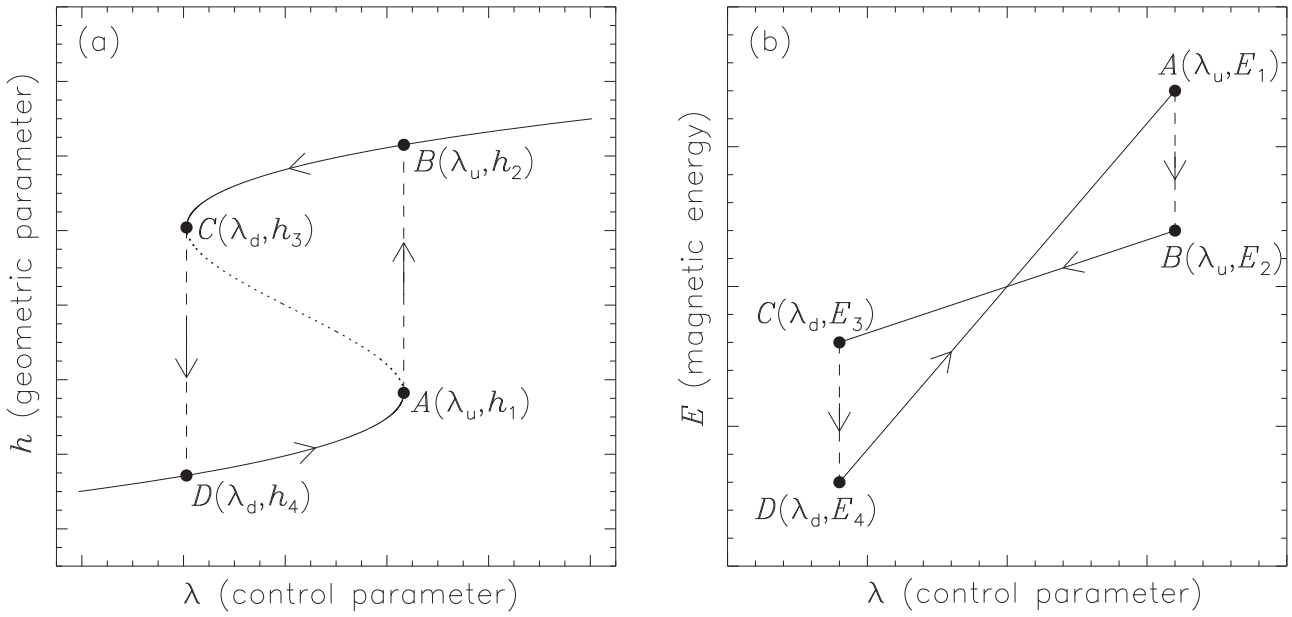

Figure 3. Schematic representations of the equilibrium solutions of the magnetic flux rope system: the profile of (a) a certain geometric parameter of the rope (h) and (b) the magnetic energy in the computational domain (E) vs. a certain control parameter of the system (λ). An upper catastrophe occurs at $\lambda = \lambda_u$, whereas a downward catastrophe occurs at $\lambda = \lambda_d$. The subscripts 1, 2, 3, and 4 label the state of the system immediately before and after the upward catastrophic point, and immediately before and after the downward catastrophic point, respectively. Although the jump of h is opposite in sign, the jump of E is always negative, implying a magnetic energy release for both of the two catastrophes.

From 0 to $100\tau_A$, Φ_z and Φ_p are smoothly adjusted. Note that at the beginning ($0 \sim 40\tau_A$), W is small but finite. This should result from the deviation of the system from equilibrium at the beginning caused by adjusting the control parameters. From $100\tau_A$ to $200\tau_A$, during which Φ_z and Φ_p are constant, the magnetic energy is almost constant if the upward catastrophe does not take place (Figure 4(e)), and W is almost zero accordingly (Figure 4(g)). If the upward catastrophe takes place, however, not only is magnetic energy released (Figure 4(f)), but also a significant peak value of W appears in Figure 4(h). The total work done by Ampère's force during the upward catastrophe is roughly estimated to be about $1.0 \times 10^{14}\,\mathrm{J\,m^{-1}}$, in the same order of the released magnetic energy ($\sim 10^{14}\,\mathrm{J\,m^{-1}}$). The deviation might result from the Poynting energy flow and the influence of relaxation method. Therefore, we may conclude that the magnetic energy is released primarily by the work done by Ampère's force during the upward catastrophe. For the downward catastrophe, although the deviation of the work done by Ampère's force from the released energy is larger, the basic conclusion remains the same as for the upward catastrophe: the work done by Ampère's force appears as a positive peak during the downward catastrophe.

4. DISCUSSION AND CONCLUSION

To investigate the catastrophic behavior of coronal flux ropes, we simulate the evolution of the equilibrium states associated with a flux rope in a force-free partially open bipolar field versus different control parameters. It is found that, under the force-free approximation, there is also a upward catastrophe. Furthermore, under the force-free approximation, there exists another possibility that a downward catastrophe takes place, during which a levitating flux rope may fall down to the photosphere. The evolutionary scenario represented by the control parameter might cause a catastrophe to take place. For example, the "flux-feeding" procedure, during which chromospheric fibrils rise upward and merge with the prominence above (Zhang et al. 2014), will result in varying Φ_z, and varying Φ_p could be caused by twisting or untwisting motions of the flux rope (Török et al. 2010; Liu et al. 2016). All these phenomena are possible triggers of catastrophes. The upward and downward catastrophes connect the two branches of equilibrium states so as to form a cycle. These two catastrophes are both irreversible but reproducible processes. Thus there might exist activities during which more than one catastrophe takes place: e.g., a flux rope is suspended in the corona at first, then falls back to the photosphere, and at last jumps upward, resulting in an eruptive activity.

By calculating the magnetic energy within the numerical domain, the evolution of magnetic energy is analyzed semi-quantitatively. Although the moving directions of the rope are opposite for the upward and downward catastrophes, magnetic energy is always released. The order of the released energy is rather large, comparable to a medium flare (see Section 3.2). Since there are no magnetic reconnections, magnetic energy is mainly released by the work done by Ampère's force. Our calculation demonstrates that the magnetic energy released by the work done by Ampère's force during a catastrophe is sufficient for solar eruptive activities, indicating that magnetic reconnection is not always necessary. If magnetic reconnection is included in the simulation, the eruptive speed can be significantly enhanced (Chen et al. 2007), and magnetic energy is released by both magnetic reconnection and the work done by Ampère's force.

Previous studies have proposed that an upward catastrophe can serve as an effective mechanism for solar eruptive activities. Since a catastrophe occurs via a loss of equilibrium at a critical point, it can be triggered by very small disturbances. In addition, upward catastrophes can not only account for CMEs and flares, they also provide sites for fast

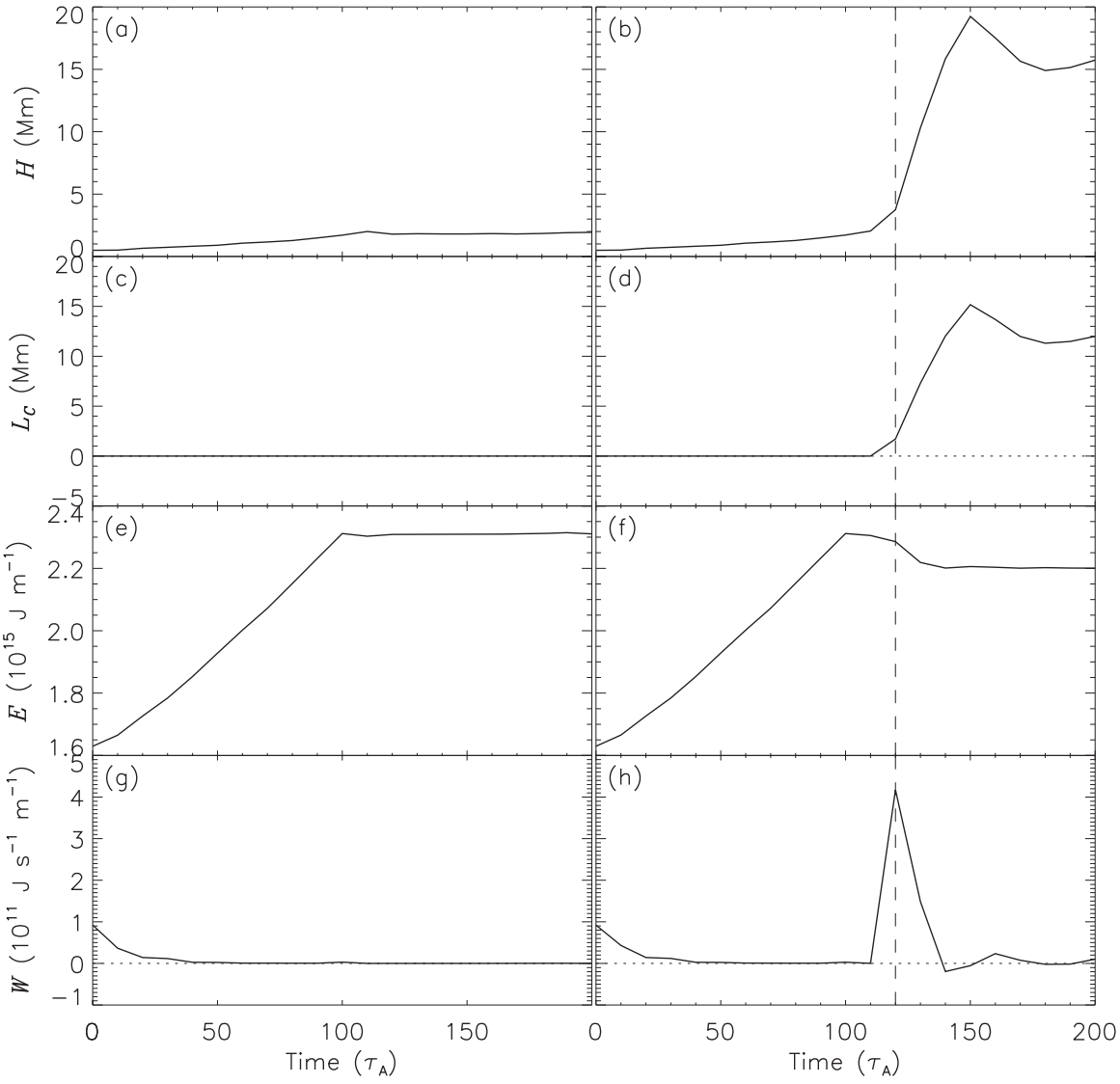

Figure 4. The temporal evolution of the height of the flux rope axis (H), the length of the current sheet below the rope (L_c), the magnetic energy in the computational domain (E), and the rate of doing work by the Ampère's force (W) during a transition from the initial state to the solution with a given annular flux of the rope, $\Phi_p = 14.9 \times 10^3$ Wb m^{-1}, are shown for the axial flux of the rope $\Phi_z = 33.4 \times 10^{10}$ Wb in the left four panels and $\Phi_z = 33.5 \times 10^{10}$ Wb in the right four panels. The axial flux changes gradually to the assigned value from $t = 0$ to $100\tau_A$ and remains invariant from $100\tau_A$ to $200\tau_A$, so as to reach a new equilibrium. The vertical dashed lines in the right panels denote the time at which the rate of doing work by Ampère's force reaches its peak value.

reconnection (Chen et al. 2007). Apart from eruptive activities, there are also energetic but non-eruptive activities, such as confined flares (Liu et al. 2014). The physical mechanism of confined flares has been discussed in many previous studies (e.g., Yang et al. 2014; Joshi et al. 2015). During a downward catastrophe, although magnetic energy is still released, the flux rope falls back to the photosphere. Therefore, a downward catastrophe might be another possible cause of energetic but non-eruptive activities. Observational evidence is still needed to confirm these conjectures.

This research is supported by Grants from NSFC 41131065, 41574165, 41421063, 41474151, and 41222031, MOEC 20113402110001, CAS Key Research Program KZZD-EW-01-4, and the Fundamental Research Funds for the Central Universities WK2080000077. R.L. acknowledges the support from the Thousand Young Talents Program of China.

REFERENCES

Amari, T., & Luciani, J. F. 1999, ApJL, 515, L81
Antiochos, S. K., DeVore, C. R., & Klimchuk, J. A. 1999, ApJ, 510, 485
Archontis, V., & Török, T. 2008, A&A, 492, L35
Benz, A. O. 2008, LRSP, 5, 1
Chen, P. F. 2011, LRSP, 8, 1
Chen, P. F., & Shibata, K. 2000, ApJ, 545, 524
Chen, Y., Hu, Y. Q., & Sun, S. J. 2007, ApJ, 665, 1421
Chen, Y., Li, G. Q., & Hu, Y. Q. 2006, ApJ, 649, 1093
Forbes, T. G. 1990, JGR, 95, 11919
Forbes, T. G., & Isenberg, P. A. 1991, ApJ, 373, 294
Forbes, T. G., & Priest, E. R. 1995, ApJ, 446, 377
Gibson, S. E., & Fan, Y. 2006, ApJL, 637, L65
Hu, Y. Q. 1989, JCoPh, 84, 441
Hu, Y. Q. 2001, SoPh, 200, 115
Hu, Y. Q. 2004, ApJ, 607, 1032
Hu, Y. Q., & Jiang, Y. W. 2001, SoPh, 203, 309
Hu, Y. Q., Li, G. Q., & Xing, X. Y. 2003, JGRA, 108, 1072
Hu, Y. Q., & Liu, W. 2000, ApJ, 540, 1119
Isenberg, P. A., Forbes, T. G., & Demoulin, P. 1993, ApJ, 417, 368
Joshi, A. D., Forbes, T. G., Park, S.-H., & Cho, K.-S. 2015, ApJ, 798, 97

Kliem, B., Lin, J., Forbes, T. G., Priest, E. R., & Török, T. 2014, ApJ, 789, 46
Kliem, B., & Török, T. 2006, PhRvL, 96, 255002
Labrosse, N., Heinzel, P., Vial, J.-C., et al. 2010, SSRv, 151, 243
Lin, J. 2004, SoPh, 219, 169
Lin, J., & van Ballegooijen, A. A. 2002, ApJ, 576, 485
Liu, R., Kliem, B., Titov, V. S., et al. 2016, ApJ, 818, 148
Liu, R., Titov, V. S., Gou, T., et al. 2014, ApJ, 790, 8
Longcope, D. W., & Forbes, T. G. 2014, SoPh, 289, 2091
Low, B. C. 1977, ApJ, 212, 234
Low, B. C. 1996, SoPh, 167, 217
Moore, R. L., Sterling, A. C., Hudson, H. S., & Lemen, J. R. 2001, ApJ, 552, 833
Priest, E. R., & Forbes, T. G. 1990, SoPh, 126, 319
Shibata, K., & Magara, T. 2011, LRSP, 8, 6
Su, Y., Surges, V., van Ballegooijen, A., DeLuca, E., & Golub, L. 2011, ApJ, 734, 53
Török, T., Berger, M. A., & Kliem, B. 2010, A&A, 516, A49
Török, T., Panasenco, O., Titov, V. S., et al. 2011, ApJL, 739, L63
Van Tend, W., & Kuperus, M. 1978, SoPh, 59, 115
Wang, Y., Zhou, Z., Shen, C., Liu, R., & Wang, S. 2015, JGRA, 120, 1543
Wang, Z., & Hu, Y.-Q. 2003, ChJAA, 3, 241
Wu, S. T., Guo, W. P., Michels, D. J., & Burlaga, L. F. 1999, JGR, 104, 14789
Yang, S., Zhang, J., & Xiang, Y. 2014, ApJL, 793, L28
Zhang, Q., Liu, R., Wang, Y., et al. 2014, ApJ, 789, 133
Zhang, Y.-Z., & Wang, J.-X. 2007, ApJ, 663, 592